

# Analysis of $E \times B$ drifts in Earth's magnetosphere during geomagnetic reversals: potential consequences for plasmasphere behavior and stability

Joe Caggiano<sup>1</sup> and Carol S Paty<sup>1</sup>

<sup>1</sup>University of Oregon

November 23, 2022

## Abstract

Geomagnetic pole reversals occur frequently throughout geologic history, although one has not yet occurred in recorded time. Magnetohydrodynamic models of Earth's core have revealed that during a reversal, the magnetic dipole moment disappears, leaving higher-order moments. Previous research examined quadrupole magnetic field topologies and quantitatively specified the magnetic equators of those topologies but did not fully examine charged particle drift motion and stability in the inner magnetosphere. Earth's closed magnetosphere is primarily dominated by two electric fields, the corotational and convection generated electric fields.  $E \times B$  drifts from these fields ultimately drives the behavior of the cold plasma of the plasmasphere. In a quadrupole-dominated magnetic field, the plasma motion generated by the  $E \times B$  drifts would be dramatically different from the classical dipole field plasma convection. Three quadrupole topologies were evaluated, and the  $E \times B$  drift was analyzed along the magnetic equators of these topologies to characterize and quantify the resultant plasma motion and evaluate the behavior, structure and stability of the plasmasphere. We also tested for plasmapause and magnetopause boundary sensitivity to magnetic field strength. The direction of the convection flow is hemispherically dependent for the  $\eta = 0$  and 0.5 quadrupole topologies, that is, the plasma in the Northern Hemisphere convects tailward, and the Southern Hemisphere convects sunward. The  $\eta = 1$  topology demonstrates evidence of strong plasmasphere erosion due to the intersection of the magnetic equators, and is particularly sensitive to reductions in magnetic field strength.

1           **Analysis of  $\mathbf{E} \times \mathbf{B}$  drifts in Earths magnetosphere**  
2           **during geomagnetic reversals: potential consequences**  
3           **for plasmasphere behavior and stability**

4                           **J. A. Caggiano<sup>1</sup> and C. S. Paty<sup>1</sup>**

5                           <sup>1</sup>Department of Earth Sciences, University of Oregon, Eugene, OR 97403.

6           **Key Points:**

- 7           • Pole reversals dramatically affect electric fields and plasmasphere stability due to  
8           changes in the topology of Earths magnetic field.
- 9           • Quadrupole magnetic field topologies generate sunward convection flows in one  
10           hemisphere, and tailward convection flows in the other hemisphere. Quadrupole  
11           topologies that exhibit rotational modulation with respect to the solar wind do  
12           not support steady-state convection and result in stronger plasmasphere erosion.
- 13           • The plasmopause and magnetopause boundary positions are sensitive to changes  
14           in magnetic field strength and are highly dependent on magnetic field topology.

## Abstract

Geomagnetic pole reversals occur frequently throughout geologic history, although one has not yet occurred in recorded time. Magnetohydrodynamic models of Earth's core have revealed that during a reversal, the magnetic dipole moment disappears, leaving higher-order moments. Previous research examined quadrupole magnetic field topologies and quantitatively specified the magnetic equators of those topologies but did not fully examine charged particle drift motion and stability in the inner magnetosphere. Earth's closed magnetosphere is primarily dominated by two electric fields, the corotational and convection generated electric fields.  $\vec{E} \times \vec{B}$  drifts from these fields ultimately drives the behavior of the cold plasma of the plasmasphere. In a quadrupole-dominated magnetic field, the plasma motion generated by the  $\vec{E} \times \vec{B}$  drifts would be dramatically different from the classical dipole field plasma convection. Three quadrupole topologies were evaluated, and the  $\vec{E} \times \vec{B}$  drift was analyzed along the magnetic equators of these topologies to characterize and quantify the resultant plasma motion and evaluate the behavior, structure and stability of the plasmasphere. We also tested for plasmapause and magnetopause boundary sensitivity to magnetic field strength. The direction of the convection flow is hemispherically dependent for the  $\eta = 0$  and  $0.5$  quadrupole topologies, that is, the plasma in the Northern Hemisphere convects tailward, and the Southern Hemisphere convects sunward. The  $\eta = 1$  topology demonstrates evidence of strong plasmasphere erosion due to the intersection of the magnetic equators, and is particularly sensitive to reductions in magnetic field strength.

## Plain Language Summary

Earth's magnetic field protects the planet from high-energy particles from the Sun. Little is known about what happens to Earth's magnetic field during a geomagnetic pole reversal, yet pole reversals occur regularly on geological timescales. Previous studies suggested that during pole reversals, Earth's magnetic field becomes more complex, taking on the appearance of magnetic quadrupoles, and the overall magnetic field strength decreases. We studied the effects a pole reversal would have on Earth's electric fields, and how that would affect the cold, atmosphere-sourced plasma in the near-Earth space environment known as the plasmasphere. We find that the stability of the plasmasphere is highly dependent on the shape of the magnetic field, and that magnetic field shapes lacking a symmetry around Earth's rotational axis lead to stronger erosion of Earth's plasmasphere, and leaves Earth's atmosphere more vulnerable to changes in magnetic field strength.

## 1 Introduction

Geomagnetic pole reversals occur consistently on Earth through geologic time scales, the latest reversal occurring approximately 781,000 years ago (Lowrie & Kent, 1983; Singer & Coe, 2019). Pole reversals, and even geomagnetic excursions, are thought to have profound effects on Earth's climate, biosphere and other surface processes (Cooper et al., 2021). However, little is known about the topology of Earth's magnetic field during a pole reversal process. Magnetohydrodynamic (MHD) geodynamo modelling of the Earth's core by Glatzmaier and Roberts (1995) has shown that during the relatively brief time period of a pole reversal the dipole moment of the magnetic field tends to disappear in favor of higher-order magnetic moments. Of the higher-order magnetic moments, the quadrupole moment decays the least with respect to distance from Earth and is therefore thought to dominate the magnetic field (Vogt & Glassmeier, 2000).

Understanding the influence of quadrupole magnetic moments on magnetospheric dynamics in general will help provide insight into Earth's magnetosphere during a pole reversal, as well as the present-day magnetospheres of other planets within the Solar System. While a pure quadrupole magnetic field has not yet been observed in a planetary body, many of the planets in our Solar System, such as Mercury, Uranus and Neptune, possess signifi-

64 cant quadrupole moments (Takahashi & Tsunakawa, 2019; Connerney & Ness, 1987; Ness  
 65 & Neubauer, 1989). For simplicity and convenience, the magnetic fields of said planetary  
 66 bodies are typically represented as dipole moments that are offset from the planet’s center  
 67 and tilted with respect to the planetary rotation axis. However, in terms of alluding to  
 68 generation mechanisms the fields are more accurately described as a combination of dipole  
 69 and quadrupole moments. Describing the importance and influence of strong quadrupole  
 70 moments is critical for a realistic understanding of planetary magnetospheric dynamics, es-  
 71 pecially in the inner magnetosphere where the higher order magnetic moments are strongest.

72 Vogt and Glassmeier (2000) derived magnetic field equations and magnetic equators for  
 73 three symmetric quadrupole topologies (Figure 1) and demonstrated that magnetospheric  
 74 plasma dynamics could behave quite differently during a pole reversal than during a normal  
 75 dipole-dominated magnetosphere. However, the scope of Vogt and Glassmeier (2000) only  
 76 extended to mapping of magnetic equipotential lines on the magnetic equators of these  
 77 quadrupole fields in order to explore the bounce motion of plasma particles in the near-  
 78 Earth environment. Their study did not consider the effects of electric fields on drifting  
 79 plasma.

80 The nature of magnetospheric convection has a significant effect on the motion of low-  
 81 energy plasma in the inner magnetosphere (Kavanaugh et al., 1968). This effect is mainly  
 82 driven by  $\vec{E} \times \vec{B}$  drifts associated with the planetary magnetic field and the local electric  
 83 fields. The main electric fields are the corotational electric field caused by the rotation  
 84 of Earth’s intrinsic magnetic field and the convection electric field is generated from the  
 85 magnetospheric convection due to the interactions of Earth’s magnetosphere with the solar  
 86 wind (Nishida, 1966). Volland (1973) and Stern (1974) semi-empirically derived an ana-  
 87 lytical model for the convection electric field for a dipole field by calculating the  $-\vec{v} \times \vec{B}$   
 88 electric potential generated by the solar wind across the poles, and extending the poten-  
 89 tial across the magnetic equator where closed-field convection occurs in a dipole dominated  
 90 magnetosphere.

91 Vogt et al. (2004) studied tail currents in the same quadrupole magnetic fields using the  
 92 BATS-R-US single-fluid MHD model. The results from their ideal MHD model were quite  
 93 remarkable in the sense that the model produced a convection profile of Earths magneto-  
 94 sphere that is dramatically different from the dipole magnetospheric convection that we see  
 95 today. However, the unconventional nature of magnetospheric convection in the quadrupole  
 96 field was largely unaddressed by the Vogt et al. (2004) study.

97 In this study, we assess the Volland-Stern magnetospheric potential model validity  
 98 for a quadrupole magnetosphere. We also examine the affect of the quadrupole field on  
 99 magnetospheric convection and analyze the corotational and convection electric fields and  
 100 their associated  $\vec{E} \times \vec{B}$  drift trajectories for several quadrupole magnetic field topologies and  
 101 use the results to infer the stability of Earths plasmasphere in the event of a pole reversal.

## 102 2 Methods

### 103 2.1 Magnetic Quadrupole Topologies

104 The quadrupole magnetic field topologies are derived using spherical harmonics. Fol-  
 105 lowing the derivation from Vogt and Glassmeier (2000), the scalar potential of a magnetic  
 106 quadrupole is expressed as:

$$107 \Psi = \frac{1}{2} \sum_{i,j=1}^3 Q_{ij} \frac{x_i x_j}{r^5} \quad (1)$$

108 Where  $\vec{r}$  is the radius from the center of the Earth and  $Q_{ij}$  is the quadrupole tensor, defined  
 109 as:

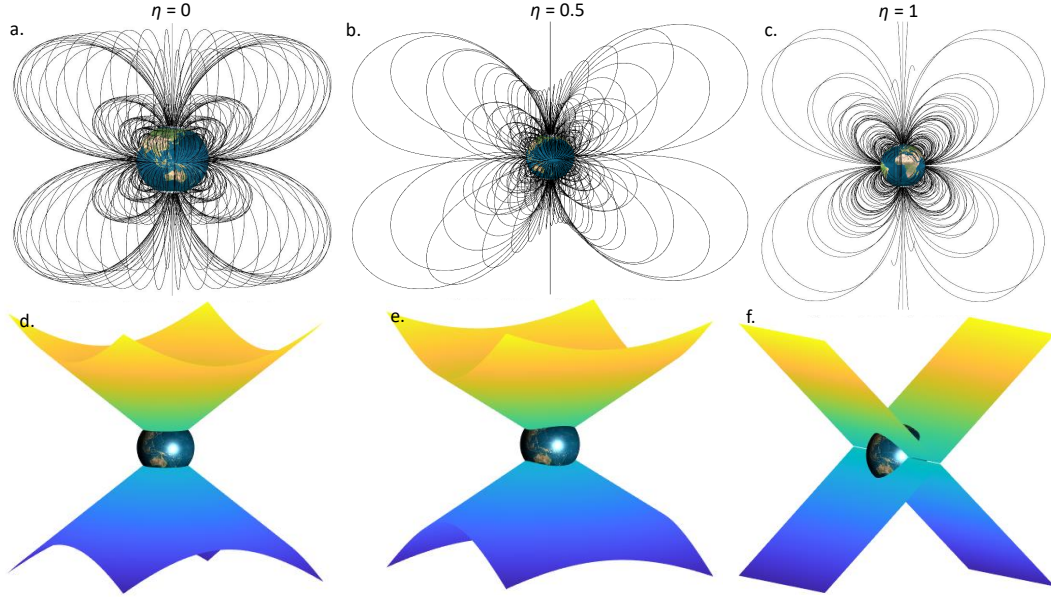


**Figure 1.** Magnetic quadrupole topologies used in the study. (a) Quadrupole field using the  $\eta = 0$  shape parameter, (b) using the  $\eta = 0.5$  shape parameter and (c) using the  $\eta = 1$  shape parameter. (d-f) Magnetic equatorial surfaces for each quadrupole topology, respectively. For the purposes of illustration, the magnetic equatorial surfaces are rotated 25 degrees to show asymmetries.

$$Q_{ij} = q \cdot \begin{pmatrix} -\frac{1-\eta}{2} & 0 & 0 \\ 0 & -\frac{1+\eta}{2} & 0 \\ 0 & 0 & 1 \end{pmatrix} \quad (2)$$

In (2),  $q$  is a scaling parameter, which for this study is set equal to 1. The shape parameter term,  $\eta$ , is what drives the differences in topologies. The  $\eta$  parameter, defined in detail by Vogt and Glassmeier (2000), is a ratio of Schmidt coefficients from the spherical harmonic expansion of the quadrupole scalar potential such that:

$$\eta = \frac{\sqrt{3}g_2^2}{g_2^0} \quad (3)$$

For the purposes of this study, we used the values 0, 0.5 and 1 for  $\eta$  to explore a wide range of quadrupole topologies. Negative values of  $\eta$  are not explored because they present the same geometry as positive values but with reversed magnetic moments. The magnetic field equations are determined for each shape parameter by taking the negative gradient of (1):

$$\vec{B} = -\nabla\Psi \quad (4)$$

Equation (4) delineates the magnetic fields for the shape parameters specified above. These magnetic fields are visualized in Figure 1. Our magnetic fields are defined so the magnetic field axis is aligned with Earth's rotational axis. This alignment is performed as a simplifying assumption that is reasonable for Earth, and allows for direct comparison to the Volland (1973) and Stern (1974) convection potential derivations, which make the same assumption.

128 The magnetic equator is defined as a surface or set of surfaces where the magnetic field  
129 gradient reaches a local minimum. This is quantitatively defined as:

$$130 \quad \vec{B}^T(\nabla\vec{B})\vec{B} = 0 \quad (5)$$

131 The equatorial surfaces produced are shown in Figure 1d-f.

## 132 2.2 Electric Fields and $\mathbf{E} \times \mathbf{B}$ Drifts

133 As the Earth rotates, the magnetic field rotates with it. This generates a  $-\vec{v} \times \vec{B}$   
134 corotational electric field around earth. The corotational electric field is defined as:

$$135 \quad \vec{E}_{CR} = \vec{\Omega} \times \vec{r} \times \vec{B} \quad (6)$$

136 where  $\vec{\Omega}$  is the angular velocity vector of the Earth in the direction of the rotation axis,  $\vec{r}$  is  
137 the position vector from the center of the Earth, and  $\vec{B}$  is the magnetic field (Maus, 2017).

138 The convection electric field is a  $-\vec{v} \times \vec{B}$  electric field brought on by the sunward flow  
139 of Earths magnetic field due to magnetospheric convection (Kavanaugh et al., 1968). This  
140 field exists within the closed magnetic field of Earths magnetosphere, although it is often  
141 projected on the equatorial plane of Earth since this is where the electric field is strongest  
142 due to the maximum convection velocity on this plane (Maus, 2017). The convection field  
143 is altered by the differential motion of ions and electrons around the Earth as plasma flows  
144 sunward via a shielding process. This shielding process is dependent on the plasma flux  
145 convecting around Earth, which is ultimately dependent on solar wind activity. The convec-  
146 tion electric field accounting for shielding is defined via the Volland-Stern magnetospheric  
147 potential (Volland, 1973; Stern, 1974; Maynard & Chen, 1975), and is semi-empirically  
148 derived based on the electric field generated by the interplanetary magnetic field moving  
149 across Earth’s polar caps. This electric field is projected onto the magnetic equator, and its  
150 electric potential can be written as:

$$151 \quad \Phi_{CS} = \frac{92.4}{R} - AR^N \sin \phi \quad (7)$$

152 Where R is the radial distance from Earth’s center, N is a parameter that is optimally equal  
153 to 2 based on work from Stern (1974), and  $\phi$  is the angle from the subsolar point in the  
154 direction of Earth’s rotation. A is the constant shielding factor based on the solar wind  
155  $k_p$ -index, given by:

$$156 \quad A = \frac{0.045}{(1 - 0.159k_p + 0.0093k_p^2)^3} \quad (8)$$

157 This study will assume a solar wind with a  $k_p$ -index value of 4 for the purposes of direct  
158 comparison to the Volland (1973) and Stern (1974) derivations. The convection electric field  
159 is the gradient of the Volland-Stern magnetospheric potential:

$$160 \quad \vec{E}_{CS} = -\nabla\Phi_{CS} \quad (9)$$

161 These electric field equations are derived with the simplifying assumption that the  
162 magnetic equator for the dipole is located at the geographic equator. to simplify modelling  
163 efforts, the coordinate system is converted to Cartesian and defined such that  $\hat{x}$  is tail-  
164 ward (away from the Sun),  $\hat{y}$  is toward the dawn side of Earths magnetopause along the  
165 geographical equator, and  $\hat{z}$  completes the right-hand coordinate system.

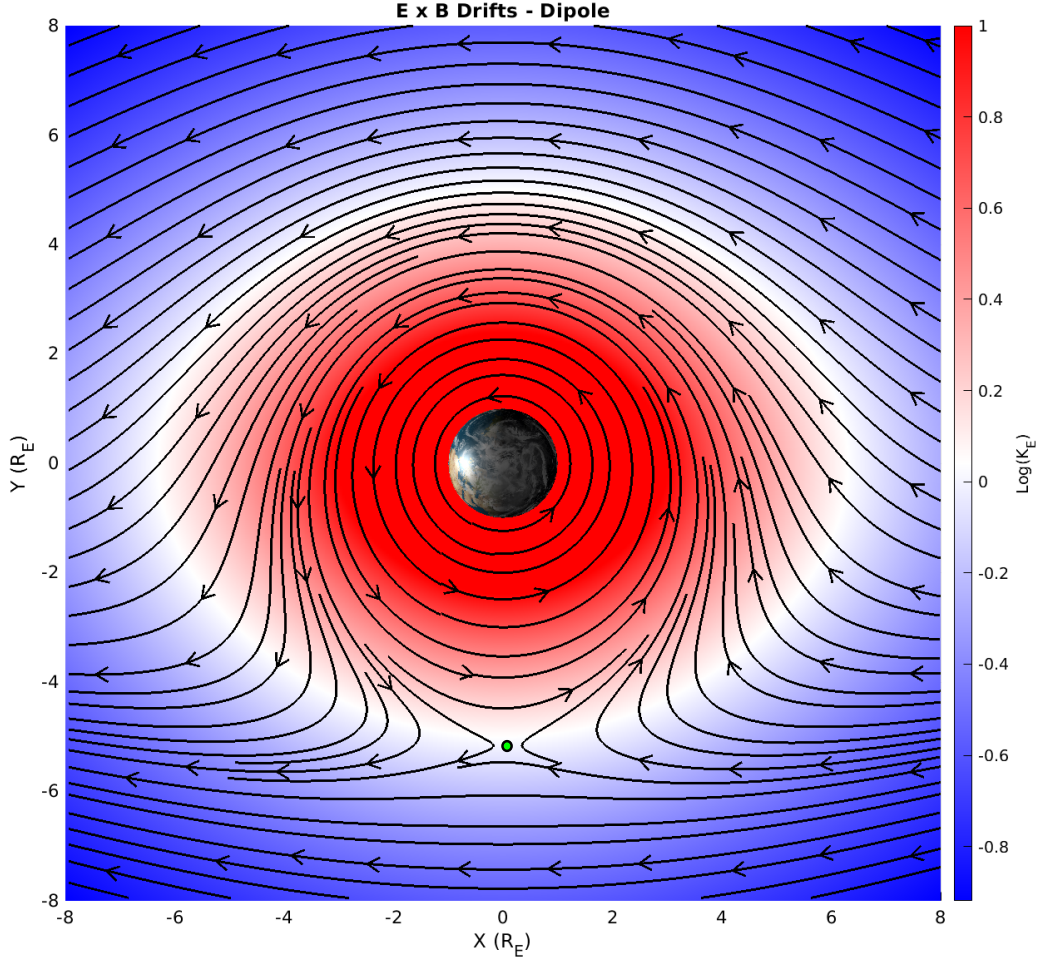


**Figure 2.** The  $\vec{E} \times \vec{B}$  drift field streamlines around Earth on the magnetic/geographic equator. All space that is red is dominated by the Corotational E-Field, and all space in blue is Convection E-Field dominated. The green dot is the location of the stagnation point.

166 Both corotational and convection electric fields are important when describing the plas-  
 167 masphere of Earth. The drift velocity of relatively cold plasma in the near-Earth environ-  
 168 nment is generated from several processes, of which the dominant mechanism is the  $\vec{E} \times \vec{B}$   
 169 drift. The  $\vec{E} \times \vec{B}$  drift velocity is quantitatively defined as:

$$170 \quad \vec{v}_D = \frac{\vec{E} \times \vec{B}}{|\vec{B}|^2} \quad (10)$$

171 The plasma motion is primarily driven by the locally dominant electric field (Baumjohann  
 172 & Treumann, 2012). Figure 2 demonstrates the influence of these electric fields on the  $\vec{E} \times \vec{B}$   
 173 drift for charged particles in a dipole magnetic field. The color bar in Figure 2 (and follow-  
 174 ing figures) denotes the regionally dominant electric field using a ratio,  $K_E$  of the relative  
 175 strength of the corotational and convection electric fields across the magnetic equator sur-  
 176 faces was calculated.

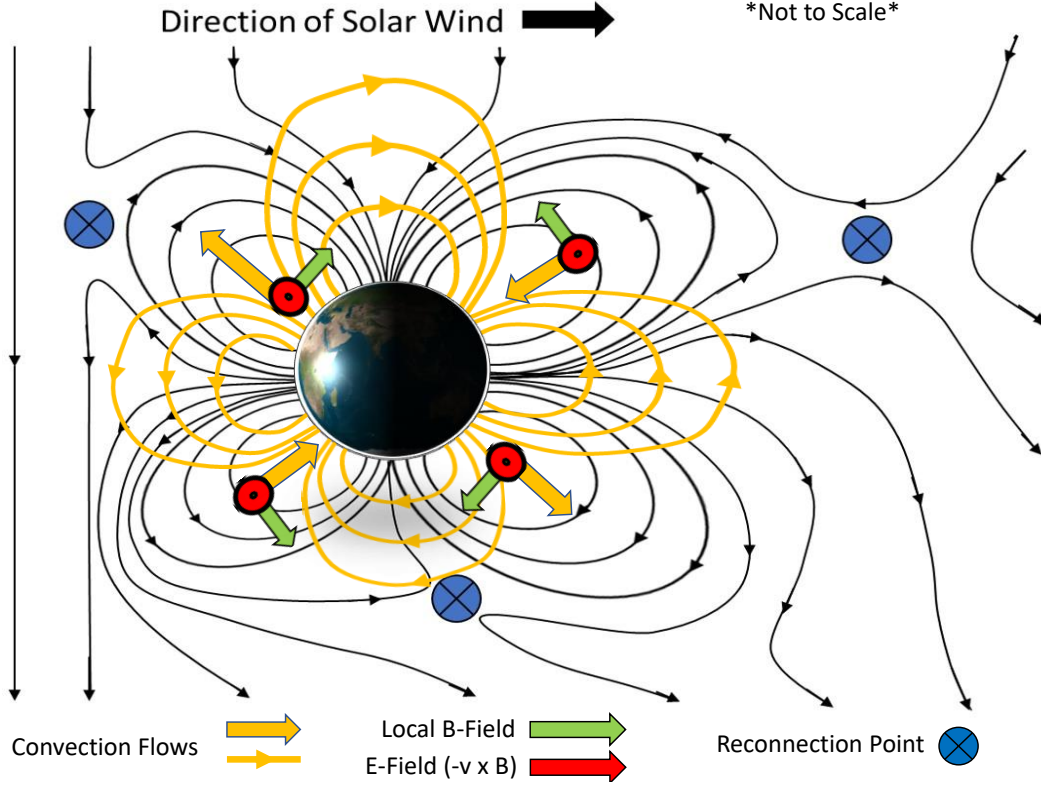


**Figure 3.** Conceptual illustration of the convection profile, flows, and calculated electric fields for a  $\eta = 0$  quadrupole magnetic field.

177

$$K_E = \frac{|\vec{E}_{CR}|}{|\vec{E}_C|} \quad (11)$$

178

179

180

181

182

183

184

185

186

187

188

The plasmopause boundary is considered to be the location on the magnetic equatorial surface where the ratio of convection and corotational electric field magnitudes is unity. In regions where the dominant electric field is corotational (red), the plasma will continue drifting around the Earth. Whereas if the plasma encounters a convection-dominated electric field (blue), it will be eroded from the plasmasphere and drift sunward towards the magnetopause. The white region indicates where the magnitudes of the convective and corotational electric fields are balanced. There is a specific point on the dusk side of Earth where the  $\vec{E} \times \vec{B}$  drifts of the corotation and convection electric fields are equal in magnitude and opposing, known as the stagnation point (Nishida, 1966; Brice, 1967; Kavanaugh et al., 1968; Baumjohann & Treumann, 2012). The stagnation points are indicated by green dots in all figures.

189

190

191

192

193

194

For the dipole magnetic field these electric fields are the most significant on the magnetic equator, which is near the geographic equator. However, in a quadrupole-dominated magnetosphere the magnetic equators are not located anywhere near the geographic equator (Vogt & Glassmeier, 2000). The magnetic equators also have curvature and complex geometries for certain quadrupole configurations (Vogt & Glassmeier, 2000) (Figure 2). The applicability of the Volland-Stern convection model must therefore be tested for a quadrupole.

### 2.3 Volland-Stern Magnetospheric Potential in a Quadrupole

Given the dipole-dependence of the Volland-Stern Magnetospheric Potential derivation, the question arises whether this convection model is useful for a quadrupole magnetosphere. This concern is addressed by examining the nature of the convection flows in a quadrupole magnetosphere. Figure 3 illustrates a conceptual map in the X-Z plane of a magnetic quadrupole field convecting while interacting with the solar wind with a southward interplanetary magnetic field. The convection and reconnection points in Figure 4 demonstrate that the quadrupole field can be divided into two hemispheric convection regions. One region shows magnetic reconnection occurring at the sunward magnetopause and in the magnetotail, which indicates open style convection. The other hemisphere reconnects with the solar wind tailward of the magnetospheric cusp, indicating a closed style convection region. Qualitative evaluation of the local  $-\vec{v} \times \vec{B}$  electric fields for the quadrupole  $\eta = 0$  reveals that the electric field and resultant  $\vec{E} \times \vec{B}$  drift velocities are in the same direction that the Volland-Stern model predicts when applied to a quadrupole at all points in the evaluated space. A derivation of the general solution of the convection electric field is available in the Appendix.

### 2.4 Variable Field Strength

Several studies have suggested that the maximum surface field strength will decrease by approximately one order of magnitude (Glassmeier & Buchert, 2004; Siscoe & Sibek, 1980; Ulte-Geurard & Achache, 1995; Vogt et al., 2004). However, given the lack of observational constraint on changes to overall magnetic field strength during a pole reversal, we explored the sensitivity of the dipole and quadrupole plasmaspheres to changes in magnetic field strength to understand how the plasmasphere erodes with smaller magnetic field strengths. To do this, the surface magnetic field strength was evaluated at 0.05, 0.1, 0.2, 0.5, 1, 2, 5, and 10 times the present-day surface magnetic field strength of 31200 nT (Baumjohann & Treumann, 2012). The plasmopause location was then found along the magnetic equators of the Earth for each magnetic configuration and surface strength.

## 3 Results

Each magnetic quadrupole topology was tested by plotting streamlines tracing the  $\vec{E} \times \vec{B}$  drift patterns along the magnetic equatorial surfaces, which are shaded based on the dominant electric field along the equatorial surfaces.

Figure 4 (Top) illustrates the  $\vec{E} \times \vec{B}$  and electric field visualization for the quadrupole field calculated with the  $\eta = 0$  shape parameter. The figure shows that Earth has two separate magnetic equator surfaces, and the  $\vec{E} \times \vec{B}$  drift patterns in convection dominated regions are structured similarly. However, because the magnetospheric convection flows are opposite along the equatorial surfaces in each hemisphere, the  $\vec{E} \times \vec{B}$  drifts for each hemisphere in the convection electric field region are travelling in opposite directions relative to each other. The plasma drift in the corotationally-dominated electric field regions continue to drift in the corotational direction. However, since each hemisphere of the plasmasphere encounters convection in opposite directions at the magnetic equators, two stagnation points appear on opposite sides of Earth on each magnetic equatorial surface.

A similar structure of opposing convection flows in each hemisphere regions is apparent for the  $\eta = 0.5$  configuration (Figure 4 Bottom). The convection fields are also typical compared to the  $\eta = 0$  topology. The corotational fields in this scenario are stable, albeit elongated due to the nature of the magnetic field topology. Due to the time dependent nature of a non-axisymmetric quadrupole, the elongated field rotates with the Earth. This implies that the stagnation points will oscillate radially and latitudinally relative to Earth. However, the closed nature of the corotational streamlines indicates that no enhancement of plasmasphere erosion is created from the oscillation.

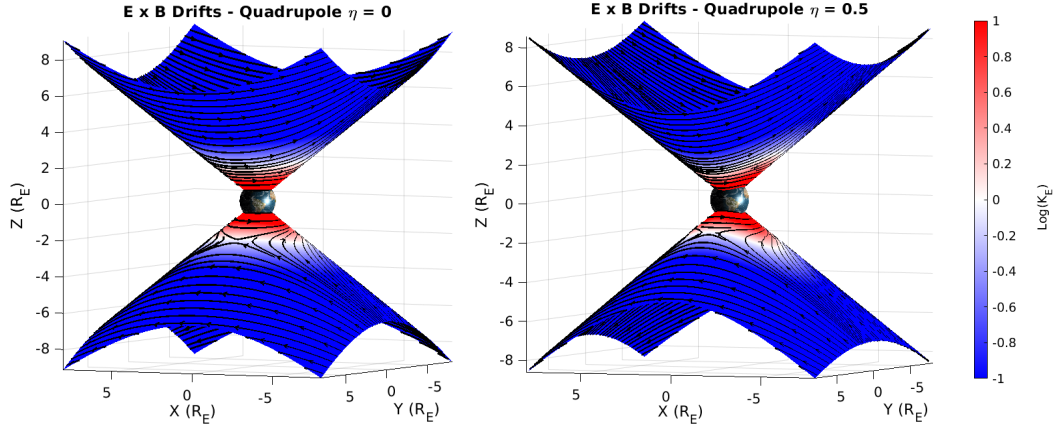


**Figure 4.**  $\vec{E} \times \vec{B}$  streamlines along the magnetic equators for  $\eta = 0$  (Left) and  $\eta = 0.5$  (Right). The colors denote whether the region is in a corotational or convection dominated electric field. Note the reversal of  $\vec{B}$  convection flows on each equatorial surface.

244 The  $\eta = 1$  topology (Figure 4) yields the most striking departure from canonical drift  
 245 motion. For certain points in the rotation of Earth where the axis of equatorial surface  
 246 convergence is oriented parallel/anti-parallel to the solar wind direction (Figure 4 - Top)  
 247 the stagnation points are configured similarly to the  $\eta = 0$  and 0.5 topologies in that each  
 248 stagnation point is present on opposite sides of the planet for each hemisphere. The hemi-  
 249 spheric regions also convect in opposite directions similarly to the other topologies. The  
 250 main feature of interest, however, is the behavior of the drifts at the convergence zone of the  
 251 two magnetic equators. The corotational electric field becomes significantly weaker with  
 252 proximity to the magnetic equatorial surface convergence, causing the area to be mainly  
 253 convection-dominated. Figure 5 shows a top-down view of the  $\eta = 1$  drift configuration.  
 254 This figure shows that when the corotationally-dominated plasma approaches the magnetic  
 255 equator convergence zone, most of the plasma enters a convection electric field dominated  
 256 area and is eroded away. This implies that a large portion of the plasmasphere would not  
 257 survive a single drift period before being eroded away and is therefore unstable except at  
 258 very low altitudes.

259 Because the  $\eta = 1$  topology also rotates with Earth, the orientation of the field relative  
 260 to the convection field is time dependent. This implies that the the axis of equatorial surface  
 261 convergence will be periodically parallel and perpendicular to the magnetic convection  
 262 flow. Figure 4 (Bottom) illustrates that when the the axis of equatorial surface convergence  
 263 is perpendicular to the solar wind direction, the stagnation points disappear since no region  
 264 exists where the corotational and convection  $\vec{E} \times \vec{B}$  drifts directly oppose each other.  
 265 The time dependent nature of  $\eta = 1$  also causes the convection field to completely change  
 266 directions in a time dependent matter, which is analyzed further in the discussion.

## 267 4 Discussion and Conclusions

268 The topology changes in the  $\vec{E} \times \vec{B}$  fields indicate a significant change in the structure of  
 269 the plasmasphere from the current dipole case. The streamlines mapped in Figure 4 indicate  
 270 that the plasmasphere tracks along the magnetic equatorial surfaces, but each hemisphere  
 271 is governed by opposing convection flows in the  $\eta = 0$  and  $\eta = 0.5$  cases. This was not the  
 272 case for the  $\eta = 1$  quadrupole, where the intersecting magnetic equators caused a significant  
 273 reduction in the corotational electric field strength. This causes a large portion of the  
 274 plasmasphere to erode into the convective field regime at this location. Therefore, the  $\eta =$

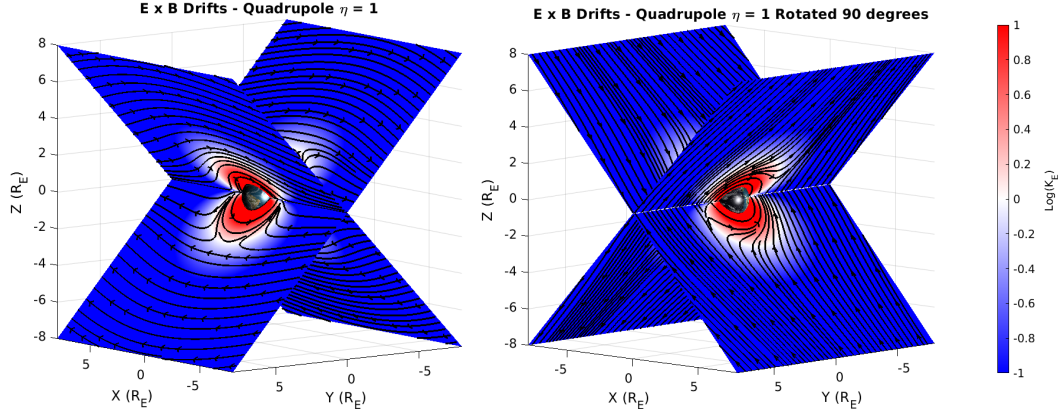


**Figure 5.** (Left)  $\vec{E} \times \vec{B}$  streamlines along the magnetic equators for  $\eta = 1$ . The colors denote whether the region is on a corotation or convection field dominated region. (Right)  $\vec{E} \times \vec{B}$  streamlines for the  $\eta = 1$  magnetic field 6 hours later. Note the decrease of corotational domination where the equatorial surfaces converge.

275 1 geometry does not support a substantial plasmasphere because most of the material does  
 276 not remain stable in the plasmasphere for more than one half of a drift orbit.

277 Development of a steady-state convection model for the quadrupole geometries is only  
 278 feasible for the  $\eta = 0$  case, due to the axisymmetry of the magnetic field. However, the  
 279 non-axisymmetry and time dependent nature of the convection flows in  $\eta = 0.5$  and 1 makes  
 280 the quantitative derivation of a steady-state convection model impossible to calculate. The  
 281 magnitude and orientation of magnetospheric convection changes periodically with rotation  
 282 of the planet. While the  $\eta = 0.5$

283 While this study presents a simplified, analytical solution to study plasmopause sta-  
 284 bility during a magnetic pole reversal, it does not account for dynamic effects such as  
 285 magnetospheric compression, changes to the solar wind or plasmasphere erosion due to ge-  
 286 omagnetic disturbances. To constrain the consequences of variable field strength of the  
 287 magnetic topologies, the plasmopause locations were evaluated for a range of surface field  
 288 strengths as described in Section 2.4. Figure 6 shows the minimum plasmopause radial  
 289 distance as a function of surface magnetic field strength relative to the present-day value  
 290 of 31200 nT. A standard dipole configuration produced the plasmasphere with the greatest  
 291 radial extent and requires the magnitude of the surface magnetic field to be reduced by  
 292 approximately two orders of magnitude for the plasmopause to become completely unsta-  
 293 ble and disappear. The quadrupole fields  $\eta = 0$  and  $\eta = 0.5$  demonstrated a significantly  
 294 weaker plasmasphere than a dipole but were still robust in that they required a similar  
 295 reduction in magnetic field strength as the dipole for the plasmasphere to disappear com-  
 296 pletely. The  $\eta = 1$  quadrupole, produced by far the most anemic plasmasphere, with a very  
 297 close plasmopause at the magnetic equator convergence zone. At the modern-day magnetic  
 298 field strength, the plasmopause is less than 1 Earth radius away from the surface. The sur-  
 299 face field strength would only need to decrease to 1/4 of the current magnetic field strength  
 300 for the plasmasphere to become completely unstable and disappear.

301 For a more complete exploration of the magnetic field strength parameter space, the  
 302 sunward magnetopause boundary was located for each of the magnetic topologies (Figure 6).  
 303 The magnetopause calculation assumed an average solar wind of 10 protons/cm<sup>3</sup> travelling  
 304 at 450 km/s. To get the most conservative magnetopause boundary estimate, the dynamic  
 305 pressure from the solar wind was aligned with the magnetic equators for each magnetic field  
 306 topology. This eliminated any obliqueness to the force balance, and pushed the magne-

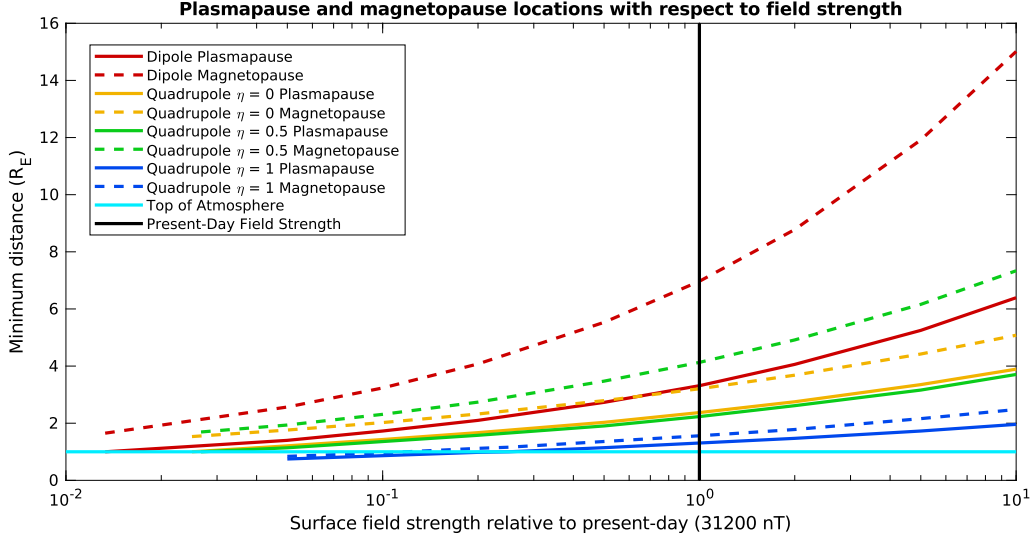


**Figure 6.** Plasmopause boundaries (Solid Lines) and the sunward magnetopause boundary (Dashed Lines) for each magnetic field topology at varying surface field strengths. The top of the atmosphere (Cyan Line at the Bottom) and the current field strength (Vertical Black Line) are also displayed.

307 topause boundary as close to Earth as possible. The calculated magnetopauses were found  
 308 to be farther away from Earth than the plasmopause boundaries, which demonstrated that  
 309 the plasmaspheres generated by the quadrupoles would be stable for magnetospheres com-  
 310 pressed by standard solar wind conditions. For the  $\eta = 1$  geometry when the field was less  
 311 than  $1/5$  of its current strength the plasmopause and magnetopause boundaries are pushed  
 312 below Earth’s surface. If the magnetic field strength decreases by an order of magnitude as  
 313 suggested in Section 2.4, and the magnetic field resembles an  $\eta = 1$  configuration, the Earth  
 314 and existing space-based assets will be directly exposed to the solar wind.

315 In summary, this study demonstrated the strong impact of quadrupole magnetic fields  
 316 on the  $\vec{E} \times \vec{B}$  drift and the structure and stability of the plasmasphere, highlighting the poten-  
 317 tial changes to Earth’s near space environment during a magnetic reversal and highlighting  
 318 potential differences in the dynamics of quadrupole-dominant planetary magnetospheres.

- 319 • Two of the quadrupole magnetic field topologies ( $\eta = 0, 0.5$ ) create two plasmasphere  
 320 regions around the corresponding magnetic equatorial surfaces. One is effected by  
 321 a sunward magnetospheric convection, and the other by a tailward magnetospheric  
 322 convection. There are also oppositely located stagnation points for each magnetic  
 323 equator.
- 324 • The  $\eta = 1$  quadrupole topology produces a weak plasmasphere that erodes signifi-  
 325 cantly at the magnetic equator intersections. This causes the plasmasphere to become  
 326 unstable since most of the plasma does not survive a single orbit around the planet.
- 327 • The axisymmetric  $\eta = 0$  Quadrupole field is the only field topology that allows for  
 328 derivation of a steady-state convection model. The other field topologies have time-  
 329 dependent convection magnitudes and orientations, and thus can never achieve a  
 330 steady state.
- 331 • The effect of changes to magnetic field strength on the plasmaphere and magneto-  
 332 sphere boundaries are strongly dependent on magnetic field topology.

333 The analytical solutions and sensitivity analysis presented in this paper provide in-  
 334 sight into to understanding the stability of the plasmasphere during magnetic reversals.  
 335 We found that the structure of the plasmasphere and sensitivity of the plasmasphere to  
 336 changes in the magnetic field strength are very dependent on the topology of the magnetic  
 337 field present during the reversal process. These characteristics deviate dramatically from  
 338 the canonical present-day dipole plasmasphere. However, we do not examine the dynamic  
 339 response of the magnetosphere to variability in the solar wind, and leave the implementation  
 340 of a 3-dimensional plasma dynamic simulation to fully characterize the Earth's near-space  
 341 environment to a future paper.

## 342 5 Appendix: Derivation of Volland-Stern Convection Potential

343 Volland (1973) and Stern (1974) semi-empirically derived the Convection electric poten-  
 344 tial using Euler potentials, which are scalar functions that characterize a plane perpendicular  
 345 to the magnetic field at any given point in space such that:

$$346 \quad \nabla\alpha \times \nabla\beta = \vec{B} \quad (12)$$

347 Where  $\alpha$  and  $\beta$  are the Euler potentials of the magnetic field which represent two scalar  
 348 functions that are orthogonal to each other and capable of describing the , and  $\vec{B}$  is the  
 349 magnetic field. Given the innate perpendicularity of the Euler potentials, they also satisfy  
 350 the following conditions:

$$351 \quad \nabla\alpha \cdot \vec{B} = 0 \quad (13)$$

$$352 \quad \nabla\beta \cdot \vec{B} = 0 \quad (14)$$

353 The above equations are quasi-linear partial differential equations. This also implies  
 354 that the Euler potentials are unique general solutions to the same quasilinear partial dif-  
 355 ferential equations. For an axisymmetric magnetic field, the convection electric field and  
 356  $\vec{E} \times \vec{B}$  drift field are assumed to be orthogonal to the magnetic field, and thus may also  
 357 serve as representations of the gradients of the Euler potentials  $\alpha$  and  $\beta$  as shown below.

$$358 \quad \vec{E} \cdot \vec{B} = 0 \quad (15)$$

$$359 \quad \left(\frac{\vec{E} \times \vec{B}}{B^2}\right) \cdot \vec{B} = 0 \quad (16)$$

360 This relationship indicates that  $\alpha$  and  $\beta$  represent the scalar potentials of the convection  
 361 electric field and the  $\vec{E} \times \vec{B}$  drift fields. Our study departs from the Volland (1973) and  
 362 Stern (1974) derivations by calculating the general solutions for the  $\eta = 0$  quadrupole instead  
 363 of a magnetic dipole. Solving the quasilinear partial differential equations for each Euler  
 364 potential in the  $\eta = 0$  topology produces the following general solutions:

$$365 \quad \alpha = C_1 \frac{y}{x} \quad (17)$$

$$366 \quad \beta = \ln \frac{(x^2 + y^2 + z^2)^{5/2}}{x^2 z} \quad (18)$$

367 The gradients of these general solutions reveal patterns very similar to the convection  
 368 electric fields and  $\vec{E} \times \vec{B}$  fields anticipated from previous research for the quadrupole field  
 369 with shape parameter  $\eta = 0$  (Figure A). The convection electric field vectors and  $\vec{E} \times \vec{B}$   
 370 matches what is predicted from the illustration in figure 3.

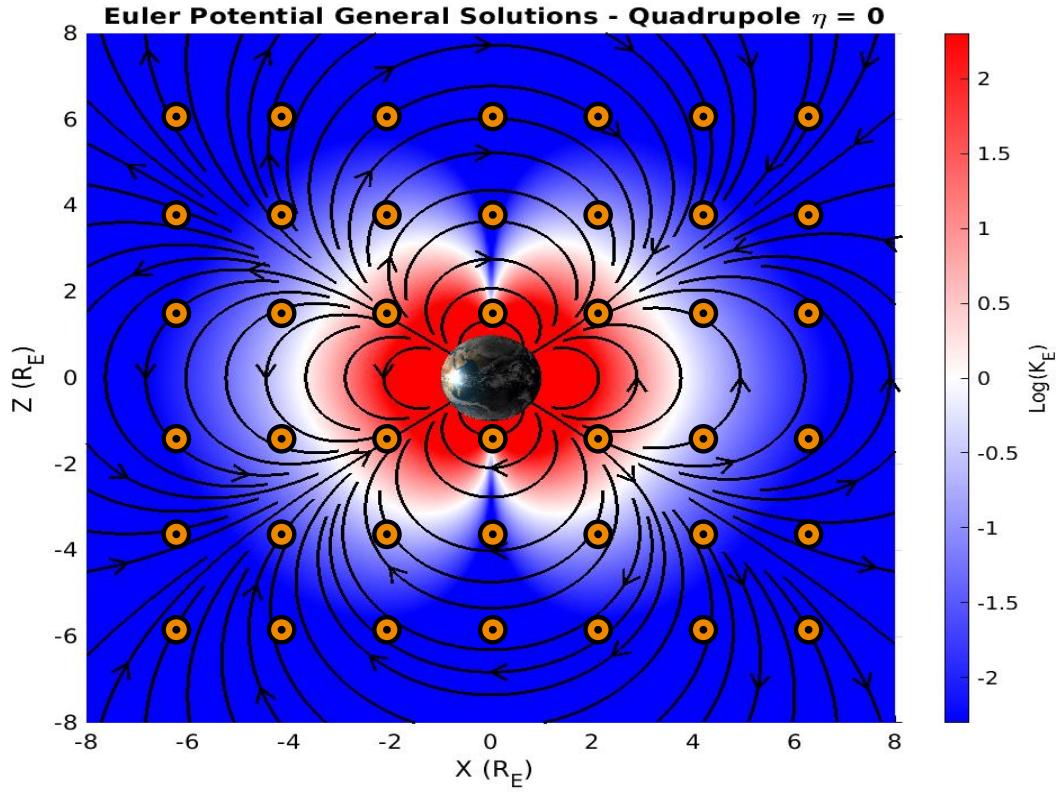


**Figure A.** General solutions for the Euler potentials. Black streamlines correspond to the  $\vec{E} \times \vec{B}$  Euler potentials, and the orange vectors pointing out of the figure are the  $\vec{E}$  Euler potentials. Colormap indicates the dominant electric field. Note the similarity of the  $\vec{E} \times \vec{B}$  and  $\vec{E}$  streamlines to those illustrated in Figure 3.

371 Solving for the particular solutions to the differential equations above, which correspond  
 372 to the scalar potentials for the convection electric field and the  $\vec{E} \times \vec{B}$  drift fields, requires  
 373 knowledge of simplifying boundary conditions. The Volland (1973) and Stern (1974) deriva-  
 374 tions opted to rely on an empirical derivation based on observational data for their dipole  
 375 case. However, no such luxury exists for the magnetic quadrupole case at this time. This  
 376 makes the derivation of the particular solutions for the scalar potentials impossible without  
 377 making bold simplifying assumptions. However, given how well the general solutions fit the  
 378 hypothesized convection model as-is, the particular solutions would only serve to slightly  
 379 refine the scalar potential structures.

### 380 Acknowledgments

381 Data sharing is not applicable to this article as no datasets were generated or analysed  
 382 during the current study. The authors would like to thank the University of Oregon for  
 383 funding this study via a First-Year Fellowship. There are no real or perceived conflicts of  
 384 interests amongst the authors, financially or otherwise. The authors would also like to thank  
 385 P. Regensburger, A. Olsen, A. Broz and M. Styczinski for their valuable commentary which  
 386 led to the improvement of this paper.

### 387 References

- 388 Baumjohann, W., & Treumann, R. A. (2012). *Basic space plasma physics*. London: Imperial  
 389 Coll. Press.
- 390 Brice, N. M. (1967). Bulk motion of the magnetosphere. *J. Geophys. Res.*, *72*, 5193-5211.
- 391 Connerney, M. H. A., J. E. P., & Ness, N. F. (1987). The magnetic field of uranus. *JGR*  
 392 *Space Physics*, *92*, 15329-15336.
- 393 Cooper, A., et al. (2021). A global environmental crisis 42,000 years ago. *Science*, *371*,  
 394 811-818.
- 395 Glassmeier, J. V. A. S., K. H., & Buchert, S. (2004). Concerning long-term geomagnetic  
 396 variations and space climatology. *Annales Geophysicae*, *22*, 3669-3677.
- 397 Glatzmaier, G. A., & Roberts, P. H. (1995). A three-dimensional self-consistent computer  
 398 simulation of a geomagnetic field reversal. *Nature*, *377*, 203-209.
- 399 Kavanaugh, L. D. J., et al. (1968). Plasma flow in the magnetosphere. *J. Geophys. Res.*,  
 400 *73*, 5511-5519.
- 401 Lowrie, W., & Kent, D. V. (1983). Geomagnetic reversal frequency since the late cretaceous.  
 402 *Earth and Planetary Science Letters*, *62*, 305-313.
- 403 Maus, S. (2017). A corotation electric field model of the earth derived from swarm satellite  
 404 magnetic field measurements. *JGR Space Physics*, *122*, 8733-8754.
- 405 Maynard, N. C., & Chen, A. J. (1975). Isolated cold plasma regions: observations and their  
 406 relation to possible production mechanisms. *J. Geophys. Res.*, *80*, 1009-1013.
- 407 Ness, M. H. A. L. F. B. J. E. P. C. R. P. L., N. F., & Neubauer, N. F. (1989). Magnetic  
 408 fields at neptune. *Science*, *246*, 1473-1478.
- 409 Nishida, A. (1966). Formation of plasmopause, or magnetospheric plasma knee, by the  
 410 combined action of magnetospheric convection and plasma escape from the tail. *J.*  
 411 *Geophys. Res.*, *71*, 5669-5679.
- 412 Singer, B. R. J. N. M., B. S., & Coe, R. S. (2019). Synchronizing volcanic, sedimentary,  
 413 and ice core records of earths last magnetic polarity reversal. *Science Advances*, *5*,  
 414 eaaw4621.
- 415 Siscoe, G. L., & Sibek, D. G. (1980). Effects of nondipole components on auroral zone  
 416 configurations during weak dipole field epochs. *J. Geophys. Res.*, *85*, 3549-3556.
- 417 Stern, D. (1974). A model of the terrestrial electric field (abstract). *Eos Trans. AGU*, *55*,  
 418 403.
- 419 Takahashi, H. S., F., & Tsunakawa, H. (2019). Mercurys anomalous magnetic field caused  
 420 by a symmetry-breaking self-regulating dynamo. *Dynamics, Structure and Evolution*  
 421 *of the Earth and Planets*, *10*, 208.

- 422 Ulte-Geurard, P., & Achache, J. (1995). Core flow instabilities and geomagnetic storms  
423 during reversals: The steens mountain impulsive field variations revisited. *Earth and*  
424 *Planetary Science Letters*, *135*, 91-99.
- 425 Vogt, J., & Glassmeier, K. H. (2000). On the location of trapped particle populations in  
426 quadrupole magnetospheres. *J. Geophys. Res.*, *105*, 13063-13071.
- 427 Vogt, J., et al. (2004). Mhd simulations of quadrupole magnetospheres. *JGR Space Physics*,  
428 *109*, A12221.
- 429 Volland, H. (1973). A semiempirical model of large-scale magnetospheric electric fields. *J.*  
430 *Geophys. Res.*, *78*, 171.